Theoretical Study of Scanning Probe Microscope Images of VTe_2

Sung Soo Park,† Jeeyoung Lee, Wang Ro Lee,‡ and Kee Hag Lee*

*Department of Chemistry, BK 21 Project, and Research Institute of Basic Sciences, Wonkwang University, Iksan, Jeonbuk 570-749, Korea. *E-mail: khlee@wonkwang.ac.kr*
†CAE Group, Central R & D Institute, Samsung Electro-Mechanics Co. Ltd., Suwon 443-803, Korea
‡Department of Industrial Chemistry, Iksan National College, Iksan, Jeonbuk 570-752, Korea
Received October 31, 2006

Ab initio periodic Hartree-Fock calculations with the full potential and minimum basis set are applied to interpretation of scanning tunneling microscope (STM) and atomic force microscope (AFM) images on 1T-VTe_2. Our results show that the simulated STM image shows asymmetry while the simulated AFM image shows the circular electron densities at the bright spots without asymmetry of electron density to agree with the experimental AFM image. The bright spots of both the STM and AFM images of VTe_2 are associated with the surface Te atoms, while the patterns of bright spots of STM and AFM images are different.

Key Words : Scanning tunneling microscope image, Atomic force microscope image, IT-VTe2, Simulated STM and AFM images, *Ab initio* method

Introduction

Recently Scanning Probe Microscopes (SPMs) techniques including Scanning Tunneling Microscope (STM) and Atomic Force Microscope (AFM) have been applied to examine the surfaces of various solid materials.[1] Layered materials, such as transition metal chalcogenides and graphite, are especially attractive as STM substrates for atomic scale imaging.

In the past decade, the experiments and theoretical interpretations in STM and AFM image of transition metal chalcogenides have developed rapidly because these compounds are found to possess a rich structural chemistry and a wide variety of unusual physical properties.[2-4] The application of layered materials includes superconductivity and metallic conductivity.[5] The intercalation properties of transition metal chalcogenides make it possible to extend the present knowledge about intercalation materials such as battery.[6]

The CdI_2 type of 1T-MX_2 (M = transition metal, X = chalcogen) have layers of composition MX_2, which are constructed from MX_6 octahedra by sharing their edges.[7] In each MX_2 layer, a slab of metal atoms is sandwiched between two slabs of chalcogen atoms, and the metal atoms of an undistorted MX_2 layer form a hexagonal lattice. The CdI_2 type 1T-MX_2 phases with different d electron counts from d^1 to d^3 exhibit various M-M clustering patterns.[7-12] These phenomena often referred to as charge density waves (CDW).[4,12] Therefore, metal chalcogenides are attractive for AFM and STM study because individual layers are held by weak van der Waal's (VDW) interactions. The experimental images and theoretical interpretation of total electron density and partial electron density based on Extended Hückel Tight Binding (EHTB) method of STM and AFM are reported for 1T-TaX2 (X = S, Se).[4]

The several crystal structure of VTe_2 is reported by distortion pattern at various temperature[6,13]: VTe_2 has a CdI_2 type structure above the transition temperature of 482 K, while the structure is monoclinic with space group $C_{2/m}$ below 482 K. The single crystal structures for MTe_2 (M = Ta, Nb, V) are observed by AFM experiments.[14] The observed AFM images for MTe_2 (M = Ta, V) were analyzed by calculating the total electron density plots on the basis of EHTB method.[15] The electronic structures for the CdI_2-type layered transition metal chalcogenides [TiX_2 (X = S, Se, Te), MTe_2 (M = V, Nb, Ta)] are calculated by Extended Hückel Tight Binding (EHTB) method.[16]

In the present work, we analyze the AFM and STM images of the layered monoclinic 1T-VTe_2, by using *ab initio* Periodic Hartree-Fock calculations in the CRYSTAL95 program.[17]

Calculations

We used *ab initio* periodic Hartree-Fock (PHF) calculations with the minimum basis set in the CRYSTAL95 program to study a monoclinic ($C_{2/m}$) VTe_2 slab model with two layers. The periodic Hartree-Fock (PHF) method systematically expands the band structure, whereas the density functional theory (DFT) systematically underestimates band gaps and band widths.[5] The computer code CRYSTAL95 is nowadays one of the standard tools for theoretical investigations in the field of material science to explain chemical and physical properties.

Applying a small bias voltage V between the tip and the sample yields a tunneling current. The ideal STM would have the greatest possible resolution and would measure the intrinsic properties of unperturbed surfaces rather than the properties of the joint surface-tip interface. A tip whose potential and wave functions were arbitrarily chosen would best achieve this ideal condition. In that case, Tersoff and Hamann[18] have considered the limit of the point probe. In the small bias voltage limit, the tunneling conductance, σ is

$$\sigma \propto \rho_{STM}(r, V) \tag{1}$$

where

$$\rho_{STM}(r, V) \equiv \int_{E_{F-eV}}^{E_F} dE\, \sigma(r, E) \tag{2}$$

and

$$\rho(r, E) \equiv \Sigma_v |\psi_v(r)|^2 \delta(E_v - E) \tag{3}$$

where r is in the position of the center of curvature of the tip s state, E_F is the Fermi energy, $\rho(r, E)$ is the surface local density of states (LDOS) of the bare surface at the center of the tip $r = (x, y, z)$ and $\psi_v(r)$ are the electron eigenstates of the unperturbed surface with corresponding energy E_v. For a periodic system, the sum of the v state is a sum of the bands and an integral of the k spacing spanning the irreducible part of the Brillouin zone. In CRYSTAL95, a regular mesh of interpolating points is used for performing the numerical integration in the reciprocal space. The details of the k integration scheme can be found in ref 19. The implied assumptions are that the description of the relevant tip states is given by a locally spherical potential well with a constant density of states where it approaches nearest to the surface with a constant density of states, and that the tunneling matrix element is independent of the lateral tip position for a constant tip-to-position and also is independent of the bias voltage V in the narrow energy region [$E_F \pm$ eV, E_F).

The calculation of STM charge density, $\rho_{STM}(r, V)$ is performed by sampling the k-space region near the Fermi surface in the irreducible part of surface Brillouin zone (BZ). Not all the k points contribute to $\rho_{STM}(r, V)$, because the portion of the band structure sampled by the STM is very small for typical tunneling voltage below ~1 V. In contact mode AFM measurements, all the electrons of the surface atoms are involved in the repulsive interactions with the tip, so that the AFM image is described by the total electron density plot $\rho_{AFM}(r)$ of the surface.

Here, we calculate the STM charge density within bias voltage 1.0 V at tip-to-surface separation of 1.0 Å. And we calculate the AFM charge density at tip-to-surface separation of 1.0 Å. The crystal structure of VTe_2 is chosen from ref. 6.

Results and Discussion

The STM and AFM images are simulated. Here we calculate STM charge densities $\rho_{STM}(r, V)$ defined in Eq. (2) and AFM charge densities $\rho_{AFM}(r)$. In other words, the STM charge density is described by the partial electron density, while the AFM charge density is described by the total electron density. Due to the phase transition of hexagonal 1T-VTe_2 (Figure 1) to monoclinic 1T-VTe_2 (Figures 2 and 3) by temperature, each monoclinic 1T-VTe_2 (thereafter referred to VTe_2) layer has two non-equivalent V atoms and three non-equivalent Te atoms[8] which form the ribbon chain. Figure 2 shows a top projection view in the *ab* plane of a single VTe_2 layer. Figure 3 shows a side projection view in the *ac* plane

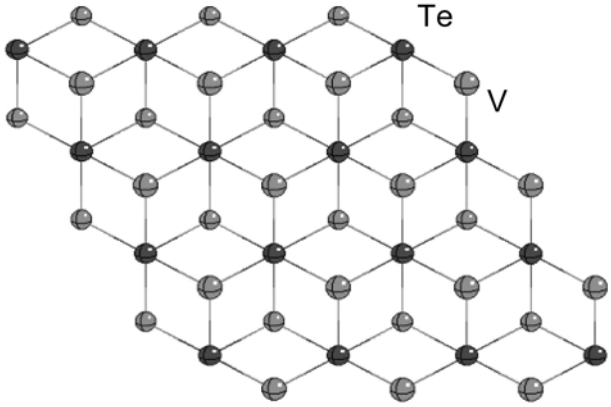

Figure 1. Schematic projection view of undistorted 1T-MX_2 (ideal CdI_2 type structure).

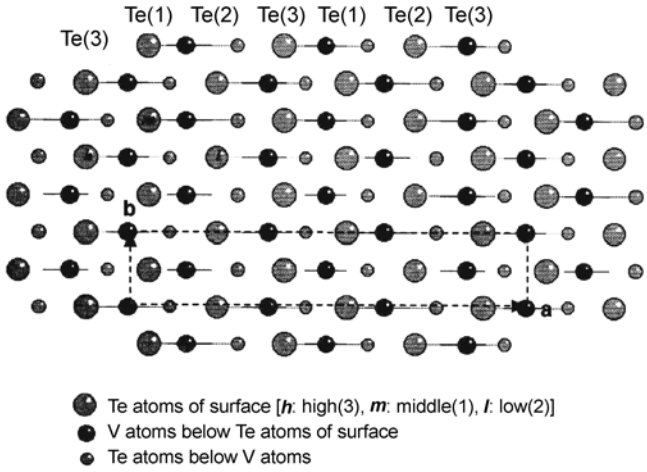

Figure 2. (001) surface of monoclinic VTe_2.

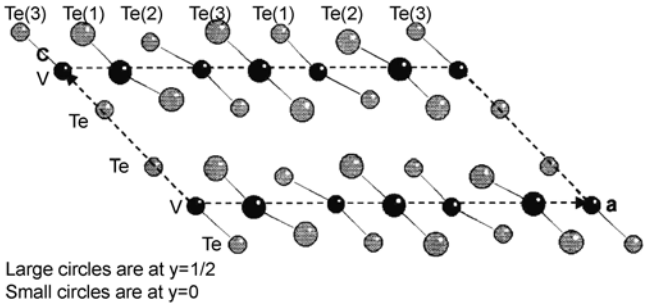

Figure 3. Projection of the structure on the (010) plane of monoclinic VTe_2.

of two adjacent VTe_2 layer along the ribbon chains which run parallel to the b-direction.

As shown in Table 1, the Te(3) atoms protrude the highest on the surface, and they lie higher than the Te(1) and Te(2) atoms by 0.488 Å and 0.086 Å, respectively. Figure 4 shows the $\rho_{AFM}(r)$ plot that has the electron density distribution on the *ab*-plane surface. In each unit cell of the $\rho_{AFM}(r)$, the electron density of the Te atom decreases in the order; Te(3) > Te(2) > Te(1). This is consistent with the finding that the distances of the surface Te atoms to the tip are increasing in the order; Te(3) < Te(2) < Te(1). Consequently the $\rho_{AFM}(r)$

Table 1. Atomic distances (Å) of VTe_2 with monoclinic structure C2/m

	Exp.	calc. (1)	calc. (2)
V(1)-V(2)	3.316(8)	3.316	3.318
V(2)-V(2)	4.32(1)	4.316	4.318
M-X distances in the centric octahedron			
V(1)-Te(1)	2.718(2)	2.718	2.718
V(1)-Te(3)	2.743(5)	2.743	2.740
M-X distances in the acentric octahedron			
V(2)-Te(1)	2.58(1)	2.583	2.58
V(2)-Te(2)	2.733(5)	2.732	2.734
V(2)-Te(2)	2.79(1)	2.790	2.789
V(2)-Te(3)	2.661(4)	2.660	2.661
X-X distances parallel to layers			
Te(1)-Te(2)	3.744(5)	3.742	3.744
Te(2)-Te(3)	3.737(5)	3.738	3.741
Te(1)-Te(3)	3.492(5)	3.492	3.494
X-X distances between to layers			
Te(1)-Te(1)	3.59(3)	3.590	3.588
Te(1)-Te(2)	3.907(6)	3.907	3.901
Te(2)-Te(3)	3.778(3)	3.778	3.776
Te(3)-Te(3)	3.595(6)	3.595	3.591
X-X distances vertical to layers			
Te(1)-Te(3)		4.077	4.075
Te(1)-Te(3)		4.198	4.193
Te(2)-Te(2)		3.447	3.443
Te(2)-Te(3)		3.947	3.946

In calc. (1), unit cell parameters: a = 18.984, b = 3.5947, c = 9.069, β = 134.62° (*J. of Solid State Chem.* **1984**, *53*, 415).[13] In calc. (2), unit cell parameters: a = 18.992, b = 3.5982, c = 9.0585, β = 134.64° (*J. of Material Chem.* **1993**, *3*, 1271).[6]

plot of Figure 4 predicts that the bright spots of the AFM images are caused by the surface Te atoms. This plot is presented by the same pattern consisting of the previous experimental image and theoretical calculation.[11] Figure 5 shows for the atomic scale STM image of VTe_2 which is characterized by rows of bright spots.

It is very difficult that we observe the STM image of VTe_2, but we can show rearrangement of high electron density in experimental result. The $\rho_{STM}(r, V)$ plot of the ab-plane (Figure 5) is considerably different from the $\rho_{AFM}(r)$ plot of Figure 4. The partial electron density on Te(1) and Te(3) atom is not spherical but represents in-plane 5p-orbital density. The crystal structure obtained from X-ray diffraction experiment which interlayer Te-Te distance of *ab* plane is about 3.6 Å whereas the distance between high electron density sites is about 2 Å to b-direction in the preliminary STM image experiment.[20] Our calculation reveals the $\rho_{STM}(r, V)$ plot which has a unit cell of rectangle of about 3.6 Å to *a*-direction and about 2.0 Å to *b*-direction. Thus, our calculation would be useful to explain qualitatively the preliminary image of STM experiment. But the vacuum STM image for VTe_2 is not obtained yet, which is necessary to compare quantitatively with our STM image obtained by the simulation.

In conclusion, our calculations suggest that the bright

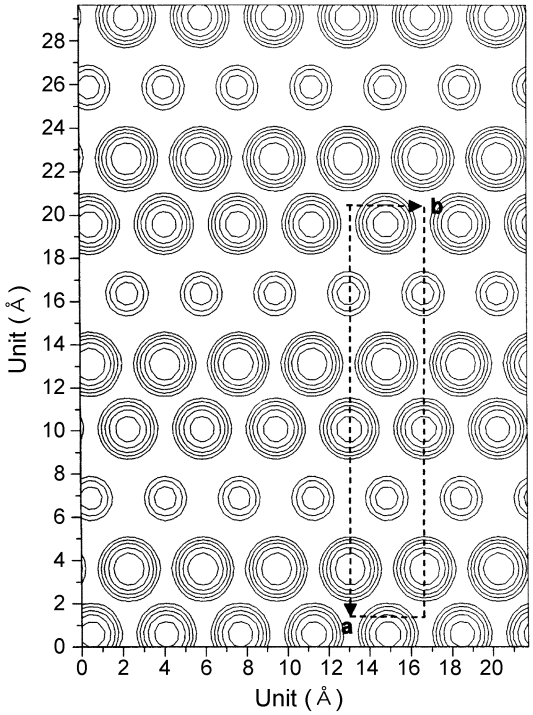

Figure 4. Contour plot of the AFM charge density in plane parallel to and 1 Å above the topmost surface layer of monoclinic VTe_2. Consecutive contours from minimum isolines (0.01) are separated up to the maximum values (0.08).

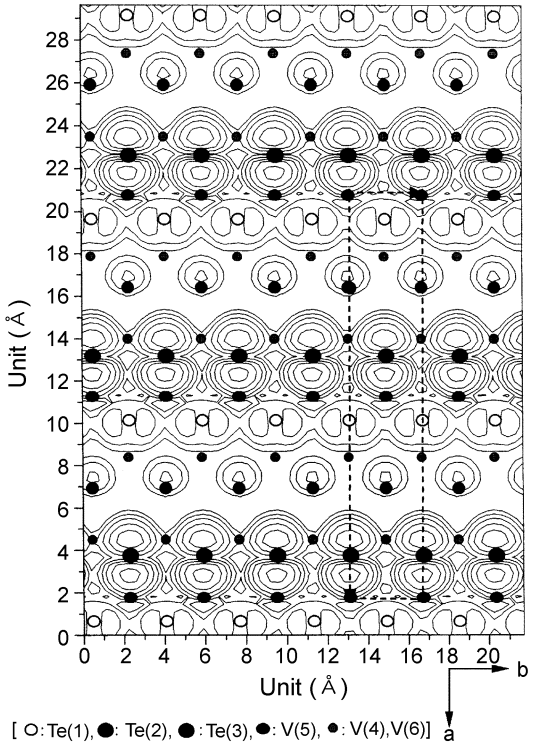

Figure 5. Contour plots of the STM charge density ρ_{STM} in plane parallel to and 1 Å above the topmost surface layer of monoclinic VTe_2. Surface result for ρ_{STM} with the tip-to-surface separation 1 Å is given for bias voltages 1.0 V. The units are 10^{-6} electrons/au^3, and consecutive contours from minimum isolines are separated with 50 steps up to 1.0×10^{-4} maximum isolines.

spots of both the STM and AFM images of VTe_2 are associated with the surface Te atoms. The STM image shows a pattern of three Te atoms of Te(1), Te(2), and Te(3) in which Te(3) has the highest electron density. Te(2) and Te(3) sites show the electron density morphology of asymmetrical dumbbell, while Te(1) sites show the electron density morphology of very weak asymmetrical dumbbell. The AFM image possesses a circle-type pattern for three kinds of Te atoms.

Acknowledgement. This work was supported by Wonkwang University in 2004. We thank Prof. H. Kang at Seoul National University for showing us his unpublished STM image of VTe_2 and stimulating discussions.

References

1. Wiesendander, R. *Scanning Probe Microscopy and Spectroscopy*; Cambridge University: Cambridge, 1994. Wiesendander, R.; Anselmetti, D. *Surface Properties and Layered Structures*; Kluwer: The netherlands, 1992. Magonov, S. N.; Whangbo, M.-H. *Surface Analysis with STM and AFM*; VCH: Weinheim: Germany, 1996. Hahn, J. R. *Bull. Korean Chem. Soc.* **2005**, *26*(7), 1071.
2. (a) Parkinson, B. A.; Ren, J.; Whangbo, M.-H. *J. Am. Chem. Soc.* **1991**, *113*, 7833. (b) Mar, A.; Jobic, S.; Ibers, J. A. *J. Am. Chem. Soc.* **1992**, *114*, 8963. (c) Ren, J.; Whangbo, M.-H.; Bengel, H.; Magonov, S. N. *J. Phys. Chem.* **1993**, *97*, 4764. (d) Ren, J.; Whangbo, M.-H.; Bengel, H.; Cantow, H. J.; Magonov, S. N. *Chem. Mater.* **1993**, *7*, 1018. (e) Ren, J.; Whangbo, M. H.; Zonnchen, P.; Rotter, H.; Cantow, H. J.; Thiele, G.; Magonov, S. N. *J. Am. Chem. Soc.* **1993**, *115*, 2495.
3. Hulliger, F. *Structural Chemistry of Layer-type Phases*; Lèvy, F., Ed.; Reidel: Dordrecht-Holland, 1976.
4. (a) Whangbo, M. H.; Canadell, E. *J. Am. Chem. Soc.* **1992**, *114*, 9587. (b) Brouwer, R.; Jellinek, F. *Physica B* **1980**, *99*, 51.
5. (a) Wilson, J. A.; DiSalbo, F. J.; Mahajan, S. *Adv. Phys.* **1975**, *24*, 117. (b) Sorgel, T.; Jansen, M. *Solid State Sci.* **2004**, *6*, 1259.
6. Williams, P. M. *Crystallography and Crystal Chemistry of Materials with Layered Structures*; Lèvy, F., Ed.; Reidel: Dordrecht-Holland, 1976.
7. *Structure Phase Transitions in Layered Transition Metal Compounds*; Motzuki, K., Ed.; Reidel: Dordrecht-Holland, 1986.
8. Doni, E.; Girlanda, R. *Electronic Structure and Electronic Transition in Layered Materials*; Grasso, V., Ed.; Reidel: Dordrecht-Holland, 1986.
9. Whangbo, M. H.; Ren, J.; Canadell, E.; Louder, D.; Pakinson, B. A.; Bengel, H.; Magonov, S. N. *J. Am. Chem. Soc.* **1993**, *115*, 3760.
10. Ishihara, Y.; Nakada, I. *Solid State Commun.* **1982**, *42*, 579.
11. Guzmán, R.; Morales, J.; Tirado, J. L. *J. Mater. Chem.* **1993**, *3*, 1271.
12. Bronsema, K. D.; Bus, G. W.; Wiegers, G. A. *J. Solid State Chem.* **1984**, *53*, 415.
13. Kim, S. J.; Park, S. J.; Oh, H. J.; Jeon, I. C.; Song, S. *Bull. Kor. Chem. Soc.* **1994**, *15*, 1098.
14. Kim, S. J.; Park, S. J.; Jeon, I. C.; Kim, C.; Pyun, C.; Yee, K. A. *J. Phys. Chem. Solids* **1997**, *58*, 659.
15. Canadell, E.; Jobic, S.; Brec, R.; Rouxel, J.; Whangbo, M. H. *J. Solid State Chem.* **1992**, *99*, 189.
16. Coleman, R. V.; Giambattista, B.; Hansma, P. K.; Johnson, A.; McNairy, W. W.; Slough, C. G. *Adv. Phys.* **1988**, *37*, 559.
17. Dovesi, R.; Saunders, V. R.; Roetti, C.; Causa, M.; Harrison, N. M.; Orlando, R.; Apra, E. *CRYSTAL95 User's Manual*; Univ. of Torino: Torino, Italy, 1996.
18. (a) Tersoff, J.; Hamann, D. R. *Phys. Rev. Lett.* **1983**, *50*, 1998. (b) Tersoff, J.; Hamann, D. R. *Phys. Rev. B* **1985**, *31*, 805. (c) Lee, K. H.; Causá, M.; Park, S. S. *J. Phys. Chem. B* **1998**, *102*, 6020. (d) Lee, K. H.; Causa, M.; Park, S. S.; Lee, C.; Suh, Y.; Eun, H. M.; Kim, D. *J. Molecular Stuc. (Theochem.)* **2000**, *297*, 301.
19. (a) Pisani, C.; Dovesi, R.; Roetti, C. *Hartree-Fock ab initio Treatment of Crystalline Systems*; Springer-Verlag: Heidelberg, 1988. (b) Pisani, C.; Apra, E.; Causa, M. *J. Quantum Chem.* **1990**, *38*, 395. (c) Pisani, C.; Apra, E.; Causa, M.; Orlando, R. *J. Quantum Chem.* **1990**, *38*, 419.
20. Unpublished result of a STM image for VTe_2 from Prof. Heon Kang at Seoul National University.